Theory of polarizable liquid crystals: Optical birefringence

Jianshu Cao[a] and B. J. Berne
Department of Chemistry and Center for Biomolecular Simulation, Columbia University, New York, New York 10027

(Received 8 February 1993; accepted 13 April 1993)

The theory of polarizable anisotropic fluids is developed on the basis of a model fluid consisting of anisotropic Drude oscillators with embedded permanent dipoles. A matrix theory is developed. The dielectric tensor is derived and a matrix Monte Carlo method is used to calculate the optical absorption and birefringence of ordered fluids.

I. INTRODUCTION

Nematic and smectic liquid crystals consist of axially symmetric molecules. A useful class of potential models for these systems is the Gaussian overlap models introduced by Berne and Pechukas.[1] These were later improved by Gay and Berne.[2] Molecular dynamics studies using these potentials have successfully simulated the nematic–isotropic and the smectic–nematic phase transitions. The phase diagram and thermodynamics of these systems have been thoroughly investigated.[3–5]

The optical properties of liquid crystals are of considerable interest. Optical birefringence is a consequence of the orientational ordering of the molecules.[6,7] It would be of interest to see if the anisotropy of optical absorption gives a signature of the orientational ordering. Can one use the absorption spectrum to discriminate between the smectic, nematic, and isotropic phases?

In this paper, we study a simple viable model of the optical properties of anisotropic liquids. We assume that the molecules are ellipsoidal and interact through the Berne–Pechukas and Gay–Berne Gaussian overlap models. Each of the ellipsoids has an implanted axially symmetric Drude oscillator embedded in it with the principal axis of the oscillator parallel to the principal axis of the Gaussian ellipsoid. The fluctuations of the Drude oscillators give rise to spontaneous dipole moments which interact with each other through dipole–dipole forces. We devise matrix methods to simulate the fluid of Drude oscillators and show how the refractive index anisotropy, the dielectric constant anisotropy, and the anisotropy of the absorption spectrum can be calculated. Monte Carlo simulations are used to study the optical properties of these fluids as a function of the orientational order parameter.

It is found that there are characteristic differences in the absorption spectra of the smectic and nematic phases. It is argued that these differences are a generic consequence of the dipole–dipole interactions and thus should be a useful signature of the spatio-orientational ordering in mesophases.

[a]In partial fulfillment of the Ph.D. in the Department of Physics, Columbia University.

II. MATRIX FORMULATION OF ANISOTROPIC LIQUIDS

The internal Hamiltonian of a single Drude molecular ellipsoid labeled i in an external field $\mathbf{E}^0$ is

$$H=H_0(\mathbf{p}_i,\dot{\mathbf{p}}_i)-\mathbf{p}_i\cdot\mathbf{E}^0=\frac{\dot{\mathbf{p}}_i\cdot\mathscr{C}^{-1}\cdot\dot{\mathbf{p}}_i}{2\alpha\omega_0^2}+\frac{\mathbf{p}_i\cdot\mathscr{C}^{-1}\cdot\mathbf{p}_i}{2\alpha}-\mathbf{p}_i\cdot\mathbf{E}_i^0, \tag{2.1}$$

where $\mathbf{p}_i$ is the instantaneous dipole and $\dot{\mathbf{p}}_i$ its associated velocities.

In the body-fixed coordinate frame in which the principal axis (the direction of the permanent dipole) is labeled z and the two other orthogonal axes are labeled x and y, the dimensionless polarizability tensor $\mathscr{C}'$ is

$$\mathscr{C}'=\frac{1}{\alpha}\begin{pmatrix}\alpha_\perp & 0 & 0\\ 0 & \alpha_\perp & 0\\ 0 & 0 & \alpha_\parallel\end{pmatrix}, \tag{2.2}$$

where $\alpha_{zz}=\alpha_\parallel$ and $\alpha_{xx}=\alpha_{yy}=\alpha_\perp$, and the polarizability matrix in the body-fixed frame is $\alpha\mathscr{C}'$. In the laboratory fixed coordinate frame, the polarizability matrix is $\alpha\mathscr{C}_i$ in which the matrix $\mathscr{C}_i$ is related to $\mathscr{C}'$ through a transformation $\mathscr{C}_i=\mathscr{R}_i^T\mathscr{C}'\mathscr{R}_i$ where the rotational matrix $\mathscr{R}_i$ is

$$\begin{aligned}\mathscr{R}_i(\theta_i,\phi_i)&=\mathscr{R}(\theta_i)\mathscr{R}(\phi_i)\\ &=\begin{bmatrix}\cos(\phi_i) & \sin(\phi_i) & 0\\ -\cos(\theta_i)\sin(\phi_i) & \cos(\theta_i)\cos(\phi_i) & -\sin(\theta_i)\\ -\sin(\theta_i)\sin(\phi_i) & \sin(\theta_i)\cos(\phi_i) & \cos(\theta_i)\end{bmatrix},\end{aligned} \tag{2.3}$$

in which θ_i and ϕ_i are the Euler angles formed by the body-fixed reference frame of molecule i with respect to the lab reference frame.

The Hamiltonian for a fluid composed of N axially symmetric Drude molecules is then

$$H=\sum_i\left[\frac{P_i^2}{2M_i}+\frac{J_i^2}{2I_i}\right]+\sum_{i>j}U_0(\mathbf{R}_{ij},\hat{u}_i,\hat{u}_j)+\sum_i H_0(\mathbf{p}_i,\dot{\mathbf{p}}_i)$$
$$-\sum_{i>j}\mathbf{p}_i\cdot\mathscr{T}_{ij}\cdot\mathbf{p}_j-\sum_i\mathbf{p}_i\cdot\mathbf{E}_i^0, \tag{2.4}$$

Downloaded 27 Mar 2001 to 18.60.2.110. Redistribution subject to AIP copyright, see http://ojps.aip.org/jcpo/jcpcr.jsp

where $\{P_i, J_i\}$ are respectively the linear and angular momenta of the molecule i, $\mathbf{R}_{ij}=\mathbf{R}_i-\mathbf{R}_j$ is the vector connecting particle i to particle j, $\hat{\mathbf{u}}$ is a unit vector specifying the orientation of the principal axis of the ellipsoid, $U_0(\mathbf{R}_{ij}, \hat{\mathbf{u}}_i, \hat{\mathbf{u}}_j)$ is the short range interaction potential between particles i and j, arising from the overlap interactions between the particles, and where the dipole–dipole propagator is

$$T_{ij}^{\mu\nu}=\frac{3R_{ij}^{\mu}R_{ij}^{\nu}-\delta^{\mu\nu}R_{ij}^2}{R^5}. \tag{2.5}$$

Tensors and matrices in this paper are represented by calligraphic symbols; $\mathscr{I}$ is the identity tensor or matrix; the upper indices $\mu\nu$ stand for coordinate components; the lower indices i or j stand for particles.

The dielectric response of polar polarizable fluids reflects two time scales—a slow time scale characterizing the reorientations of the permanent dipoles and a fast time scale characterizing the response of the embedded Drude oscillators. Thus the frequency dependent dielectric constant will reflect this separation of time scales by having low frequency bands arising from the reorientation of the permanent dipoles (rotational relaxation) and high frequency bands corresponding to charge redistribution in the molecules. The zero frequency (static) dielectric constant will of course have contributions from both of these time scales. Given the separation in time scales, the charge redistribution should rapidly follow changes in the nuclear positions. Thus the system will be well approximated by the adiabatic approximation, i.e., the Born–Oppenheimer approximation.[8,9]

In the adiabatic approximation, the nuclear degrees of freedom need not be treated as dynamical variables. Thus the conjugate momenta of the nuclear positions and orientations in Eq. (2.4) are omitted giving the Born–Oppenheimer Hamiltonian

$$H_{\mathrm{BO}}=\sum_{i>j}U_0(\mathbf{R}_{ij},\hat{u}_i,\hat{u}_j)+H_{\mathrm{DO}}, \tag{2.6}$$

where the Drude oscillator Hamiltonian is

$$H_{\mathrm{DO}}=\sum_i H_0(\mathbf{p}_i,\dot{\mathbf{p}}_i)-\sum_{i>j}\mathbf{p}_i\cdot\mathscr{T}_{ij}\cdot\mathbf{p}_j-\sum_i\mathbf{p}_i\cdot\mathbf{E}_i^0 \tag{2.7}$$

and where $\mathbf{u}_i$ and $\mathbf{u}_j$ are unit vectors specifying the orientations of molecules i and j, respectively. The first term U_0 in Eq. (2.6) determines the distribution of the nuclear configuration and the second term H_{DO} determines the dynamics of the system.

The expectation of observables $O[(R_i),(u_i),(p_i),(\dot{p}_i)]$, is

$$\langle O\rangle=\frac{\int d(R_i)d(u_i)d(p_i)d(\dot{p}_i)O[(R_i),(u_i),(p_i),(\dot{p}_i)]\exp(-H_{\mathrm{BO}}/kT)}{\int d(R_i)d(u_i)d(p_i)d(\dot{p}_i)\exp(-H_{\mathrm{BO}}/kT)}, \tag{2.8}$$

where the denominator in Eq. (2.8) is the canonical partition function Z_{BO}, in the BO approximation. It is a simple matter to express Z_{BO} as

$$Z_{\mathrm{BO}}=\int d(R_i)d(u_i)Z_{\mathrm{DO}}[(R_i),(u_i)]\times\exp\left[-\beta\sum_{i>j}U(\mathbf{R}_{ij},\hat{u}_i,\hat{u}_j)\right], \tag{2.9}$$

where $Z_{\mathrm{DO}}[(R_i),(u_i)]$ is the partition function of the Drude oscillators for a fixed nuclear configuration.

Because H_{DO} is quadratic in both (p_i) and $(\dot{p}_i)$, the multivariate Gaussian integral can be evaluated exactly, giving

$$\begin{aligned}Z_{\mathrm{DO}}[(R_i),(u_i)]&=\int d(p_i)d(\dot{p}_i)\exp(-\beta H_{\mathrm{DO}})\\&=C_N\left(\frac{1}{\det\mathscr{C}\mathscr{A}}\right)^{1/2}\exp\left[\frac{\beta\alpha}{2}(\mathbf{E}^0\cdot\mathscr{A}^{-1}\cdot\mathbf{E}^0)\right],\end{aligned} \tag{2.10}$$

where C_N is the normalization constant, the matrix $\mathscr{A}$ is given by

$$\mathscr{A}=\mathscr{C}^{-1}-\alpha\mathscr{T}, \tag{2.11}$$

and $\mathscr{C}$ is given by

$$\mathscr{C}=\begin{pmatrix}\mathscr{C}_1 & 0 & 0 & \cdots\\ 0 & \mathscr{C}_2 & 0 & \cdots\\ \vdots & \vdots & \vdots & \vdots\\ \cdots & 0 & 0 & \mathscr{C}_N\end{pmatrix}. \tag{2.12}$$

These definitions of $\mathscr{A}$ and $\mathscr{C}$ will be particularly convenient for the calculation of the electronic absorption spectra of liquid crystals.

It is simple to show that the potential of mean force for the nuclear coordinates in the BO approximation is[9]

$$W(R_i,u_i)=\sum U_0(\mathbf{R}_{ij},\hat{u}_i,\hat{u}_j)+\tfrac{1}{2}kT\ln[\det(\mathscr{A})]-\frac{\alpha}{2}\sum_{i,j}(\mathbf{E}^0\cdot\mathscr{A}^{-1}\cdot\mathbf{E}^0), \tag{2.13}$$

where the second term arises from the prefactor $(\det\mathscr{A})^{1/2}$ in Eq. (2.10).

The second term on the right-hand side in Eq. (2.13) gives the classical many-body dispersion energy of the system. In classical theory, this is small because the vibrational amplitudes of the Drude oscillators are very small $O(\sqrt{kT})$. Zero point fluctuations in quantum systems give larger amplitudes and correspondingly much larger disper-

Downloaded 27 Mar 2001 to 18.60.2.110. Redistribution subject to AIP copyright, see http://ojps.aip.org/jcpo/jcpcr.jsp

sion interactions (see Ref. 10). In simulations, only the two-body part of the dispersion interaction is usually included by incorporating it into the simple pairwise potentials, but is should be recognized that the above expression contains many-body effects to all orders.

As can be seen here and later on, all the relevant quantities can be determined by applying proper matrix techniques. In this paper and other papers of the series, these matrices are evaluated both analytically and numerically.

The frequency response functions of a system consisting of Drude oscillators is the same for classical and quantum systems because the Hamiltonian is quadratic.[11,12] A fluid of Drude oscillators driven by a monochromatic electromagnetic field $\mathbf{E}_i(\omega)e^{-i\omega t}$ obeys the set of linear equations of motion

$$\mathscr{C}_i^{-1}\frac{\ddot{\mathbf{p}}_i}{\omega_0}+\mathscr{C}_i^{-1}\mathbf{p}_i-\alpha\mathscr{T}_{ij}\mathbf{p}_j=\alpha\mathbf{E}_i(\omega)e^{-i\omega t}, \tag{2.14}$$

where ω_0 is the intrinsic frequency of the harmonic oscillator and α is the static polarizability. We make a further assumption here that although the polarizability is anisotropic, the intrinsic frequency which describes the molecular Drude oscillator is isotropic. (In reality, one should use an anisotropic Drude oscillator in which not only $\alpha_\perp \neq \alpha_\parallel$, but also the frequencies parallel and perpendicular to the principal axis of the molecule are different. This would not be difficult to incorporate.)

The particular solution of Eq. (2.14)

$$\mathbf{p}_i(t)=\alpha(\omega)\mathscr{A}^{-1}(\omega)_{ij}\mathbf{E}_j(\omega)e^{-i\omega t} \tag{2.15}$$

gives the frequency dependent response function, or the susceptibility matrix,[11–14]

$$\chi_{ij}(\omega)=\rho\alpha(\omega)\langle\mathscr{A}^{-1}(\omega)\rangle_{ij}, \tag{2.16}$$

where ρ is the density and the matrix $\mathscr{A}$ is defined as

$$\mathscr{A}(\omega)=\mathscr{C}^{-1}-\alpha(\omega)\mathscr{T} \tag{2.17}$$

the frequency dependent analog of Eq. (2.11), where $\alpha(\omega)$ is the frequency dependent polarizability

$$\alpha(\omega)=\frac{\alpha}{1-(\omega/\omega_0)^2} \tag{2.18}$$

and α is the static polarizability.

We will study cylindrically symmetrical ellipsoids with the polarizability tensor in the body-fixed frame given by Eq. (2.2). Let us write $\alpha_\parallel = a^2\times\alpha$ and $\alpha_\perp=\alpha$, so that the inverse matrix of Eq. (2.2) can be expressed as $\mathscr{C}'^{-1}=\mathscr{M}^2$, where $\mathscr{M}$ is the scaling matrix defined by

$$\mathscr{M}=\begin{pmatrix}1&0&0\\0&1&0\\0&0&1/a\end{pmatrix}. \tag{2.19}$$

The rotational matrix $\mathscr{R}$ for the whole fluid is a block diagonalized matrix

$$\mathscr{R}=\begin{pmatrix}R_1&0&0&\cdots\\0&R_2&0&\cdots\\\vdots&\vdots&\vdots&\vdots\\\cdots&0&0&R_N\end{pmatrix}, \tag{2.20}$$

where R_i is the 3×3 rotational matrix for ith molecule given in Eq. (2.3).

Since $\mathscr{C}^{-1}=\mathscr{R}^T\mathscr{C}'^{-1}\mathscr{R}=\mathscr{R}^T\mathscr{M}^2\mathscr{R}$, it follows that the matrix (2.17) can be expressed as

$$\mathscr{A}(\omega)=\mathscr{R}^T\mathscr{M}[\mathscr{I}-\alpha(\omega)\mathscr{T}']\mathscr{M}\mathscr{R}, \tag{2.21}$$

where the resulting $\mathscr{T}'$ is given by

$$\mathscr{T}'=\mathscr{M}^{-1}\mathscr{R}\mathscr{T}\mathscr{R}^T\mathscr{M}^{-1}. \tag{2.22}$$

This $\mathscr{T}'$ matrix can be easily diagonized, i.e., $\mathscr{T}'=\mathscr{S}\Lambda\mathscr{S}^{-1}$, where $\Lambda_{ij}=\lambda_i\delta_{ij}$ is the diagonal matrix, λ_i is the ith eigenvalue, and $\mathscr{S}$ is the transformation matrix. Thus

$$\mathscr{A}(\omega)=\mathscr{S}'[\mathscr{I}-\alpha(\omega)\Lambda]\mathscr{S}'^{-1}, \tag{2.23}$$

in which the $\mathscr{S}'$ matrix is

$$\mathscr{S}'=\mathscr{R}^T\mathscr{M}\mathscr{S}. \tag{2.24}$$

The spectral density matrix of the fluid is defined as

$$\mathscr{F}_{ij}(\lambda)=\langle\mathscr{S}'_{ik}\delta(\lambda-\lambda_k)\mathscr{S}'^{-1}_{kj}\rangle \tag{2.25}$$

in terms of which Eq. (2.16) becomes

$$\chi_{ij}(\omega)=\int\mathscr{F}_{ij}(\lambda)\frac{\alpha\rho}{1-(\omega/\omega_0)^2-\alpha\lambda}\,d\lambda. \tag{2.26}$$

In Eq. (2.25), the average denoted by the bracket $\langle\cdots\rangle$ is taken over the spatial and orientational configurations of the fluid determined by U_0 of Eq. (2.6). This gives the optical spectrum of unpolarized light. Here we are interested in the absorption of light polarized parallel and perpendicular to the order parameter of the liquid crystal. Therefore we define the parallel and perpendicular components of the spectral density as

$$\bar{F}_\parallel(\lambda)=\frac{\Sigma_{ij}\mathscr{F}^{zz}_{ij}(\lambda)}{N} \tag{2.27}$$

and

$$\bar{F}_\perp(\lambda)=\frac{\Sigma_{ij}[\mathscr{F}^{xx}_{ij}(\lambda)+\mathscr{F}^{yy}_{ij}(\lambda)]}{2N}, \tag{2.28}$$

where z is the spatial direction we specified. In an isotropic fluid $\bar{F}_\parallel=\bar{F}_\perp$, whereas in a liquid crystal $\bar{F}_\parallel\neq\bar{F}_\perp$.

Because the dipole–dipole interaction is long ranged, the calculations will be very sensitive to the system size and geometry and thus to the boundary conditions.[15–17] Following the discussion in the paper by de Leeuw *et al.*, in Ewald summation[17] the dipole propagator Eq. (2.5) must be replaced by Eq. (3.10) in Ref. 18. Because the Ewald summation is a function of ϵ_0, the dielectric constant of the surrounding medium, the frequency dependent response function (2.26) is also a function of ϵ_0. However, the frequency dependent dielectric constant $\epsilon(\omega)$ is an intrinsic

Downloaded 27 Mar 2001 to 18.60.2.110. Redistribution subject to AIP copyright, see http://ojps.aip.org/jcpo/jcpcr.jsp

property of the liquid which does not depend on the boundary conditions despite the fact that the boundary conditions affect the long range potential.

Consider a large spherical sample of polarizable material immersed in a medium of dielectric constant ϵ_0.[16,19] It is a standard exercise to solve the Maxwell equations for this system and obtain the frequency dependent generalization of the Kirkwood relation[15,19,20]

$$\frac{[\epsilon(\omega)-1](2\epsilon_0+1)}{\epsilon(\omega)+2\epsilon_0}=4\pi\rho\lim_{N\to\infty}\left\langle\frac{\Sigma_\mu\Sigma_{ij}\chi_{ij}^{\mu\mu}(\omega,\epsilon_0)}{3N}\right\rangle, \tag{2.29}$$

where ϵ_0 is the dielectric constant of the surrounding medium. In our simulations, the surrounding medium is taken as a perfect conductor with $\epsilon_0=\infty$.

Once the absorption spectral density function is known, we can determine the frequency dependent dielectric constant

$$\epsilon_\xi(\omega)=1+4\pi\rho\alpha\int\frac{\bar{F}_\xi(\lambda)}{1-(\omega/\omega_0)^2-\alpha\lambda} \tag{2.30}$$

and the power spectrum

$$I_\xi(\omega)=\omega\chi_\xi''(\omega)=\pi\omega\rho\alpha\bar{F}_\xi\left(\lambda=\frac{\omega_0^2-\omega^2}{\omega_0^2\alpha}\right), \tag{2.31}$$

where ξ refers to the parallel and perpendicular components and χ'' is the imaginary part of the response function which can be obtained by adding an infinitesimal imaginary part to the variable ω in Eq. (2.26) giving

$$\lim_{\eta\to0^+}\chi_\xi(\omega+i\eta)=\int\alpha\rho F_\xi(\lambda)\left\{P\frac{1}{1-(\omega/\omega_0)^2-\alpha\lambda}+i\pi\delta[1-(\omega/\omega_0)^2-\alpha\lambda]\right\}d\lambda. \tag{2.32}$$

From Eq. (2.30), we can determine the static dielectric constant $\epsilon_\xi(\omega=0)$ and the refractive index $\eta_\xi(\omega)=\sqrt{\epsilon_\xi(\omega)}$.

III. RESULTS FOR THE BERNE–PECHUKAS FLUID

The Berne–Pechukas Gaussian overlap potential takes the form of a Lennard-Jones potential[1]

$$V(\hat{u}_1,\hat{u}_2,\mathbf{r})=4\epsilon(\hat{u}_1,\hat{u}_2)\left\{\left[\frac{\sigma(\hat{u}_1,\hat{u}_2,\hat{r})}{r}\right]^{12}-\left[\frac{\sigma(\hat{u}_1,\hat{u}_2,\hat{r}}{r}\right]^6\right\}, \tag{3.1}$$

where $\hat{u}_1$ and $\hat{u}_2$ are the orientation vectors of the two molecules, $\mathbf{r}$ is a vector connecting their centers, and $\hat{r}$ is a unit vector along $\mathbf{r}$. The potential parameters ϵ and σ are the functions of the relative position and orientation of the two molecules

$$\epsilon(\hat{u}_1,\hat{u}_2)=\epsilon_0[1-\kappa^2(\hat{u}_1\cdot\hat{u}_2)^2]^{-1/2} \tag{3.2}$$

and

$$\sigma(\hat{u}_1,\hat{u}_2,\hat{r})=\sigma_0\left\{1-\frac{\kappa}{2}\left[\frac{(\hat{r}\cdot\hat{u}_1+\hat{r}\cdot\hat{u}_2)^2}{1+\kappa(\hat{u}_1\cdot\hat{u}_2)}+\frac{(\hat{r}\cdot\hat{u}_1-\hat{r}\cdot\hat{u}_2)^2}{1-\kappa(\hat{u}_1\cdot\hat{u}_2)}\right]\right\}^{1/2}, \tag{3.3}$$

where ϵ_0 and σ_0 are two constants and κ is determined by the anisotropy of the ellipsoids

$$\kappa=\frac{\sigma_\parallel^2-\sigma_\perp^2}{\sigma_\parallel^2+\sigma_\perp^2}. \tag{3.4}$$

Here $\sigma_\parallel$ is the length scale along the molecular axis and $\sigma_\perp$ is the length scale perpendicular to the axis.

The polarizability components $\alpha_\parallel$ and $\alpha_\perp$ are, respectively, proportional to the mean-square dipole fluctuation along the principal axis and one of the other symmetry axes. Thus we expect that the ratio $a^2=\alpha_\parallel/\alpha_\perp$ will scale with $\sigma_\parallel/\sigma_\perp$. Here we chose this scaling to be

$$a=\left(\frac{\sigma_\parallel}{\sigma_\perp}\right),$$

which relates the anisotropy of the polarizability to the geometry of the molecule. The actual scaling is a rather complicated problem and depends on how aromatic the molecule is. Generally the polarizability anisotropy will be considerably smaller than predicted on the basis of this scaling.

Molecular dynamics studies of anisotropic fluids of ellipsoidal molecules interacting through the overlap potential indicate that a 2D system of ellipses of axial ratio $a=3$ can exist in a stable nematic phase at densities intermediate between the solid and isotropic liquid states.[3] Similarly it has been shown that the overlap model also leads to nematic ordering in 3D systems. The isotropic–nematic phase transition must be accompanied by changes in the optical and dielectric properties. The purpose of this work is to simulate these changes.

Configurations of a Gaussian overlap fluid are generated by Monte Carlo importance sampling. Moves of the molecular position and orientation are adjusted to yield a 40%–60% acceptance rate. At the beginning of the run, following Kushick and Berne, an external electric field along the z axis is applied to the fluid. All the molecules align with the direction of the field. The field is then turned off. Initially, the body-fixed frame of all the molecules coincides with the lab frame. After the field is switched off, we determine the relaxation of the order parameter of the system. As the system is equilibrated, the order parameter reaches a plateau. The rotational order parameter measures the global orientational order and is defined by

$$\zeta=\langle P_2(\hat{u}\cdot\hat{n})\rangle, \tag{3.5}$$

where P_2 is the second order Legendre polynomial and $\hat{n}$ is the space fixed axis specified by the initial direction of molecules. ζ is monitored as the system is relaxing. At some densities, the system stays at a metastable state for some time before it reach a new plateau value. Therefore because of long relaxation times, very long runs are required before equilibrium is achieved.

Downloaded 27 Mar 2001 to 18.60.2.110. Redistribution subject to AIP copyright, see http://ojps.aip.org/jcpo/jcpcr.jsp

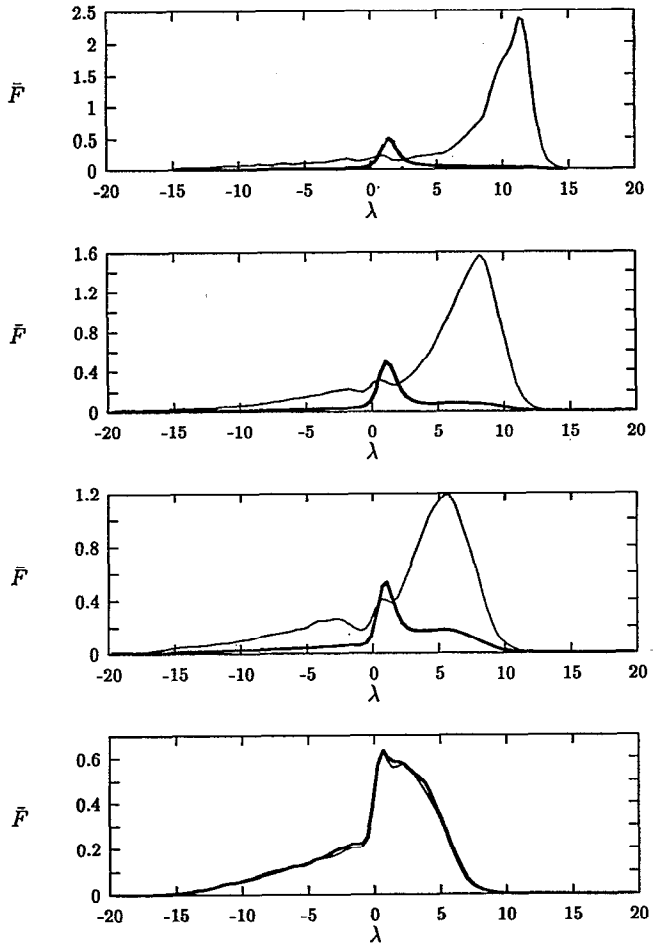

FIG. 1. The parallel component $\bar{F}_{\|}$ (the solid curve) and the perpendicular component $\bar{F}_{\perp}$ (the bold curve) of the spectral density for the Berne–Pechukas potential described in the text. The four panels from the top to the bottom correspond to reduced densities of 0.3, 0.25, 0.2, and 0.1, respectively.

The system simulated is at a reduced temperature of $kT/\epsilon=0.8$ and reduced density of $\rho^*=\rho\sigma_0^3$. The axial ratio a is taken to be 3.5. The system is composed of 108 particles. We find a transition from an isotropic system to an anisotropic system at a reduced density of 0.2 to 0.1.

The results for several densities are compared in Fig. 1. As expected, at high density the system is strongly ordered and we observe two distinct curves for $\bar{F}_{\|}$ and $\bar{F}_{\perp}$. Because the molecules are highly anisotropic, the polarization is much stronger in that direction than in the orthogonal directions. Figure 1 shows that $\bar{F}_{\|}$ is broader and more intense than $\bar{F}_{\perp}$. As the order parameter decreases with the density, the differences between these two components diminishes. When ζ approaches zero, the system becomes isotropic and $\bar{F}_{\|}$ and $\bar{F}_{\perp}$ become identical.

In Fig. 2, the perpendicular and parallel components of the static dielectric constant tensor $\epsilon_{\|,\perp}$ are plotted as a function of density. Clearly, the transition from the isotropic to the nematic phase is accompanied by a bifurcation in the dielectric constant. In the isotropic phase, the dielectric constant is a slowly increasing function of density. After the transition, the curve splits into two branches—the perpendicular component and the parallel component. In the nematic phase, the molecular principal axes align. Since $\alpha_{\|} \gg \alpha_{\perp}$, the parallel component of the static dielectric constant will increase strongly with the density; on the other hand, the perpendicular component will decrease with the density.

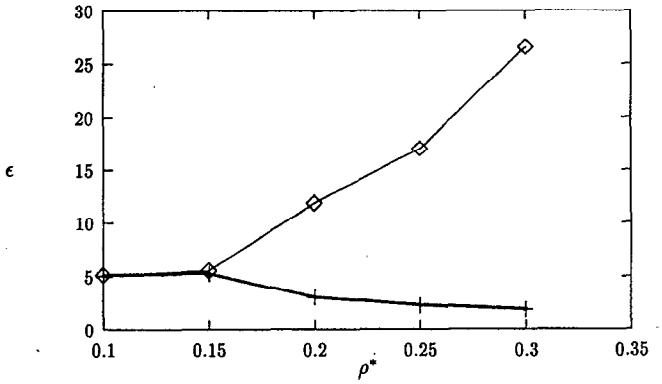

FIG. 2. The parallel component $\epsilon_{\|}$ (□) [cf. Eq. (2.27)] and perpendicular component (+) [cf. Eq. (2.28)] of the dielectric tensor as a function of density for the Berne–Pechukas fluid.

An interesting and important property of liquid crystals is their optical birefringence. The refraction index for light propagating parallel to the axis of the fluid is different from light propagating perpendicular to this direction.[6,7] This is obviously due to the anisotropy in the dielectric response function. The refractive index is related to the frequency dependent dielectric constant by $n_{\xi}(\omega) = \sqrt{\epsilon_{\xi}(\omega)}$. The birefringence can therefore be determined from Eq. (2.30).

De Jeu studied the anisotropy of the properties of liquid crystals theoretically and showed how they correlate with the orientational order parameter.[6] Let us introduce the anisotropy of the dielectric constant η as

$$\eta=\frac{\epsilon_{\|}-\epsilon_{\perp}}{\bar{\epsilon}-1}, \tag{3.6}$$

in which $\bar{\epsilon}=(\epsilon_{\perp}+2\epsilon_{\|})/3$. According to De Jeu, η should be a linear function of the second order parameter ζ. We plot η defined above as a function of the order parameter ζ from our simulations in Fig. 3. Clearly the prediction of De Jeu is completely consistent with our results. A simple symmetry argument shows that the anisotropy of a second rank tensor must be proportional to the second order Legendre polynomial which defines the order parameter (see Berne and Pecora[21]).

IV. RESULTS FOR THE GAY–BERNE MODEL

The Berne–Pechukas potential is unrealistic in that for certain orientations it is too long range. To rectify this flaw, Gay and Berne modified the Berne–Pechukas model to[2]

Downloaded 27 Mar 2001 to 18.60.2.110. Redistribution subject to AIP copyright, see http://ojps.aip.org/jcpo/jcpcr.jsp

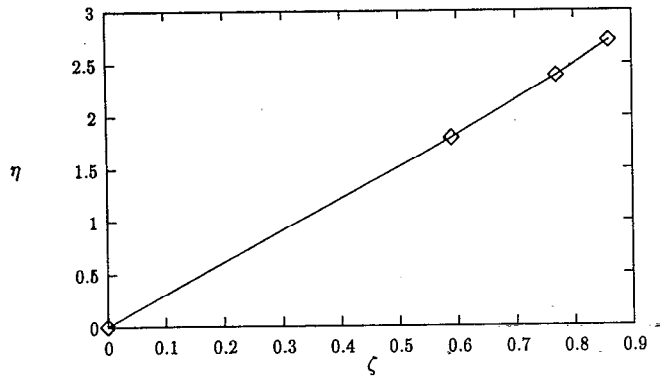

FIG. 3. η, the anisotropy of the dielectric constant defined by Eq. (3.6) as a function of order parameter for the Berne–Pechukas fluid.

$$V(\hat{u}_1,\hat{u}_2,\mathbf{r})=4\epsilon(\hat{u}_1,\hat{u}_2,\hat{r})\left[\left(\frac{1}{r-\sigma(\hat{u}_1,\hat{u}_2,\hat{r})+1}\right)^{12}-\left(\frac{1}{r-\sigma(\hat{u}_1,\hat{u}_2,\hat{r})+1}\right)^{6}\right], \tag{4.1}$$

where $\sigma(\hat{u}_1,\hat{u}_2,\hat{r})$ is still given by Eq. (3.3), but the depth parameter has the new form

$$\epsilon(\hat{u}_1,\hat{u}_2,\hat{r})=\epsilon^{\nu}(\hat{u}_1,\hat{u}_2)\epsilon'^{\mu}(\hat{u}_1,\hat{u}_2,\hat{r}), \tag{4.2}$$

where $\epsilon(\hat{u}_1,\hat{u}_2)$ is given by Eq. (3.2) and ϵ' defined by

$$\epsilon'^{\mu}(\hat{u}_1,\hat{u}_2,\hat{r})=1-\frac{\kappa'}{2}\left[\frac{(\hat{r}\cdot\hat{u}_1+\hat{r}\cdot\hat{u}_2)^2}{1+\kappa'(\hat{u}_1\cdot\hat{u}_2)}+\frac{(\hat{r}\cdot\hat{u}_1-\hat{r}\cdot\hat{u}_2)^2}{1-\kappa'(\hat{u}_1\cdot\hat{u}_2)}\right], \tag{4.3}$$

where the parameter κ' which reflects the anisotropy in the well depth is defined as

$$\kappa'=\frac{\epsilon_{\parallel}^{1/\mu}-\epsilon_{\perp}^{1/\mu}}{\epsilon_{\parallel}^{1/\mu}+\epsilon_{\perp}^{1/\mu}}, \tag{4.4}$$

in which $\epsilon_{\parallel}$ is the strength parameter along the molecular axis and $\epsilon_{\perp}$ is the strength parameter perpendicular to the axis. The Gay–Berne potential agrees well with a site–site potential. A satisfactory fit is found to the four Lennard-Jones (L-J) site–site potentials by setting $\nu=1$, $\mu=2$, the axial ratio $\sigma_{\parallel}/\sigma_{\perp}=3$, and the well-depth ratio $\epsilon_{\parallel}/\epsilon_{\perp}=3$. These parameters are chosen to model a typical mesogenic molecule.

Molecular simulation of the Gay–Berne fluid has been performed and reported in great detail. Adams *et al.*[4] found that the system exhibits a nematic to isotropic phase transition at the reduced temperature T^* between 1.7 to 1.8 and reduced density $\rho^*=0.32$. They claimed that this relatively realistic model should be of considerable value in the investigation of nematogenic behavior using computer simulation techniques.

More recently, Miguel *et al.* presented a systematic study of the phase diagram of the Gay–Berne fluid.[5] They determined the vapor–liquid coexistence region using Gibbs ensemble Monte Carlo. From the coexistence curve, they determined the critical values of the density, temperature, and pressure. The triple point was approximately located. Extensive simulations were employed to explore the rest of the phase diagram in which isotropic, nematic, and smectic phases were identified. The results indicated that above the triple point temperature $T^*\approx 0.8$, the system can form a nematic phase which under further compression becomes a smectic phase, while below the triple point temperature, the nematic phase is unstable and the isotropic liquid undergoes a direct transition to the smectic phase.

We simulated a system consisting of 256 particles interacting under the Gay–Berne potential with the parameters given above with constant volume Monte Carlo. Periodic boundary conditions and minimum image summation are employed. The interaction potential is truncated and shifted up at $r_c=4.0\sigma_0$. The trial step sizes in position and orientation are adjusted to yield an acceptance rate of 50%. We start with a low density molecular configuration and gradually compress the volume while keeping the temperature constant. We choose to study the spectrum along the isotherm at $T^*=0.5$, which is below the triple point temperature. To determine the absorption spectral densities and other equilibrium properties, 10^5 uncorrelated configurations are sampled.

Unlike simulations of the Berne–Pechukas model in the preceding section, we do not apply a weak external field to align the system initially, but instead start with a disordered system. As the whole system may rotate in space, we cannot specify a space-fixed direction as $\hat{n}$ in the calculation of the rotational order parameter of Eq. (4.2). Instead, we introduce the second rank orientational pair correlation function given as

$$G_2(|\mathbf{r}|)=\langle P_2(\hat{u}_i\cdot\hat{u}_j)\delta(\mathbf{r}_{ij}-\mathbf{r})\rangle, \tag{4.5}$$

which measures the orientational correlation as a function of the separation. In the case of the isotropic fluid, G_2 decays to zero at large r because there long-range order does not exist, but for the nematic and smectic phases, the $r\to\infty$ limit of G_2 does not vanish and is equal to the square of the order parameter ζ [cf. Eq. (3.5)].

We also determine the pair correlation function $g(r)$. In the smectic phase, the molecules form a layered structure with a spatial order along the interlayer direction and the pair correlation function of the smectic liquid exhibits pronounced peaks and structures at long distance, while the pair correlation function of the isotropic fluid and the nematic fluid shows a decaying oscillation around unity at long distances.

The smectic phase has both translational and orientational long-range order, the nematic phase has only long-range orientational order, and the isotropic liquid has neither. From the long distance behavior of $G_2(r)$ and $g(r)$, we can easily identify these phases.

In Fig. 4, we plot $G_2(r)$ and $g(r)$ at reduced densities 0.3, 0.29, 0.28, and 0.26 along the isotherm $T^*=0.5$. As was pointed out by Miguel *et al.*, as the Gay–Berne fluid is compressed from a density of 0.26–0.30, it goes from an isotropic fluid at low density directly to a smectic phase at the three higher densities. The orientational ordering sets in at a density of 0.28 as indicated by a nonvanishing order

Downloaded 27 Mar 2001 to 18.60.2.110. Redistribution subject to AIP copyright, see http://ojps.aip.org/jcpo/jcpcr.jsp

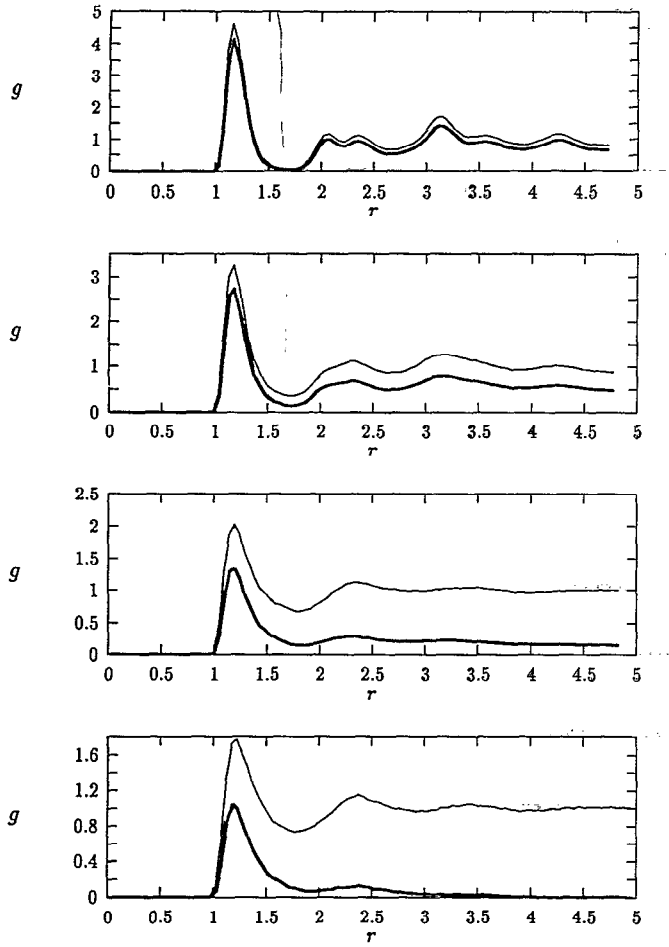

FIG. 4. The pair correlation function $g(r)$ (the solid curve) and the second rank orientational pair correlation function $G_2(r)$ defined by Eq. (4.5) (the bold curve) for the Gay–Berne fluid described in the text. The four panels from the top to the bottom correspond to the reduced densities at 0.3, 0.29, 0.28, and 0.26, respectively.

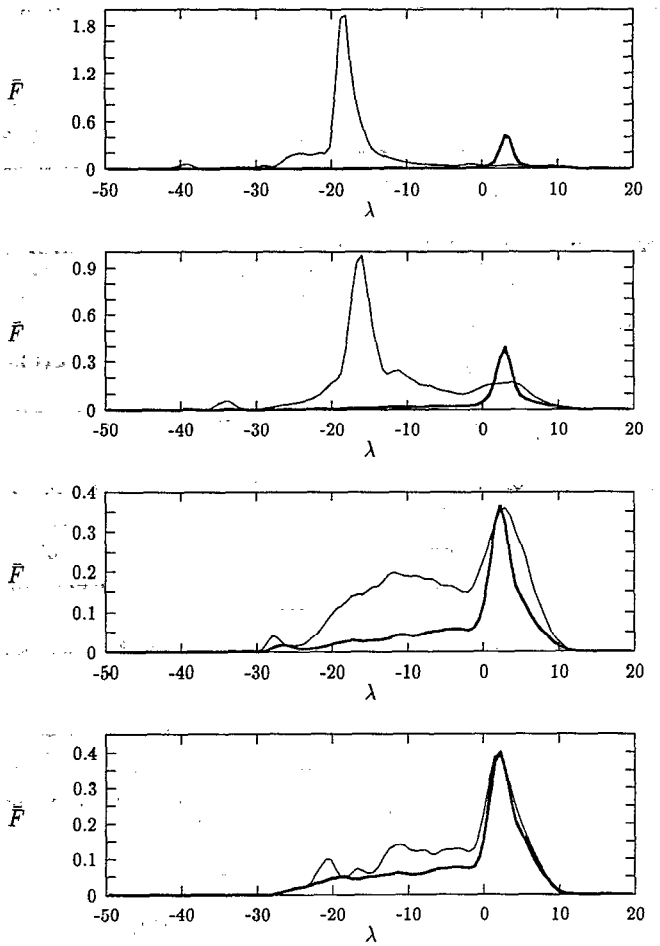

FIG. 5. The parallel component $\bar{F}_{\parallel}$ (the solid curve) and the perpendicular component $\bar{F}_{\perp}$ (the bold curve) of the spectral density function [cf. Eq. (4.6)] for the Gay–Berne fluid. The four panels from the top to the bottom correspond to the reduced densities at 0.3, 0.29, 0.28, and 0.26, respectively.

parameter. The order parameter is 0.9, 0.7, 0.4, and 0.0 for these four densities. In going from the low to the high density, $g(r)$ starts to develop structural features which demonstrate the spatial correlation typical of smectic fluids. A peak sets in at the spacing of the smectic layers. At $\rho^*=0.30$, the coincidence of $G_2(r)$ and $g(r)$ clearly indicates a well-defined alignment of the molecules, and the growth of the peak at 3.0σ indicates the formation of a layered structure. All these observations agree well with the conclusions of Miguel *et al.*

In these simulations, the ordering takes place spontaneously and it is useful to adopt a procedure for resolving observables into components parallel and perpendicular to the axis of the liquid crystal. This is done as follows: The spectral density matrix is defined as

$$\bar{F}^{\mu\nu}=\frac{\Sigma_{ij}F_{ij}^{\mu\nu}}{N}, \tag{4.6}$$

where i and j are the particle indices, and ν and μ are the coordinate indices. We diagonalize the matrix $\bar{F}$. Then the maximum eigenvalue is taken as $\bar{F}_{\parallel}$ and the average of the two other eigenvalues values is taken as $\bar{F}_{\perp}$. In Fig. 5, we plot the two components of the spectral density functions at the four densities defined above. In Fig. 6, we calculate the two components of the dielectric constant $\epsilon_{\parallel,\perp}$ using Eq. (2.30).

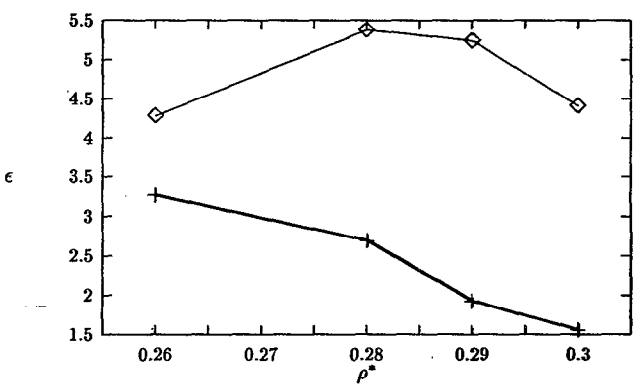

FIG. 6. The parallel component $\epsilon_{\parallel}$ (□) and perpendicular component $\epsilon_{\perp}$ (+) of the dielectric tensor for the Gay–Berne fluid as a function of reduced density.

Downloaded 27 Mar 2001 to 18.60.2.110. Redistribution subject to AIP copyright, see http://ojps.aip.org/jcpo/jcpcr.jsp

Comparing Fig. 5 with the results of the isotropic nematic phases in Fig. 1, we ascertain the following distinct characteristics of the smectic phase:

(a) A common property of the spectral density of anisotropic fluids is that the parallel component has a higher and broader peak than the perpendicular component. In the smectic phase, this prominent parallel component is blue shifted from the perpendicular component, while it is red shifted from the perpendicular component in the nematic phase. [The frequency spectrum is related to the spectral density through $\omega^2=\omega_0^2(1-\alpha\lambda)$.] This is due to the layered structure of the smectic phase. Because the distance between the layers is much larger than the distance between the molecules of the same layer, the many-body polarization of the particles in the same layer is dominant. One can solve the simple problem of three molecules in the xy plane. It is found that the zz element of the matrix $\mathcal{T}$ is opposite in sign and smaller in value than the xx or yy elements. This explains the differences of the spectral peaks between the nematic and smectic phases. This qualitative difference between the nematic and smectic phases should allow one to use the spectrum to distinguish between these different states of orientational order.

(b) In the upper two plates of Fig. 5, there are noticeable small bands besides the main peak. These small bumps probably arise from the periodicity in the z direction in the smectic phase, where there is translational disorder in the xy plane and periodicity along the z axis.

(c) In Fig. 6, $\epsilon_{\|}$ decreases with density (or order parameter). This can be attributed to the fact that the dipole–dipole interaction makes the parallel component larger than the perpendicular component, but as the smectic ordering grows stronger, the layering along the z axis becomes more pronounced thereby increasing the separations along the z axis and reducing the z–z dipole–dipole interactions without changing the dipole–dipole interaction in the xy plane.

We believe that the Gay–Berne potential gives an accurate view of the isotropic–smectic transition. The characteristic properties demonstrated in these simulations should provide general rules for smectic liquids and can be observed in experiments.

[1] B. J. Berne and P. Pechukas, J. Chem. Phys. **56**, 4213 (1972).
[2] J. G. Gay and B. J. Berne, J. Chem. Phys. **74**, 3316 (1981).
[3] J. Kushick and B. J. Berne, J. Chem. Phys. **59**, 4486 (1973).
[4] D. J. Adams, G. R. Luckhurst, and P. W. Phippen, Mol. Phys. **61**, 1575 (1987).
[5] E. De Miguel, L. F. Rull, M. K. Chalam, and K. E. Gubbins, Mol. Phys. **71**, 1223 (1990).
[6] W. H. de Jeu, *Thermotropic Liquid Crystals: Fundamentals* (Springer, New York, 1988).
[7] S. Chandraskhar, *Liquid Crystals* (Cambridge University, Cambridge, 1977).
[8] A. S. Davydov, *Quantum Mechanics* (Pergamon, New York, 1965).
[9] J. Cao and B. J. Berne, J. Chem. Phys. (in press).
[10] J. Cao and B. J. Berne, J. Chem. Phys. **97**, 8628 (1992).
[11] D. Chandler, K. S. Schweizer, and P. G. Wolynes, Phys. Rev. Lett. **49**, 1100 (1982).
[12] Z. Chen and R. Stratt, J. Chem. Phys. **95**, 2669 (1991).
[13] B. Cichocki and B. U. Felderhof, J. Chem. Phys. **90**, 4960 (1989).
[14] B. Cichocki and B. U. Felderhof, J. Chem. Phys. **92**, 6104 (1990).
[15] J. P. Hansen and I. R. McDonald, *Theory of Simple Fluids* (Academic, New York, 1986).
[16] B. Cichocki, B. U. Felderhof, and K. Kinsen, Phys. Rev. A **39**, 5350 (1989).
[17] S. W. de Leeuw, J. W. Perram, and E. R. Smith, Proc. R. Soc. London Ser. A **373**, 27 (1980).
[18] J. Cao and B. J. Berne, J. Chem. Phys. (submitted).
[19] G. Stell, G. N. Patey, and J. S. Hoye, Adv. Chem. Phys. **48**, 183 (1981).
[20] B. J. Alder and E. L. Pollock, Annu. Rev. Phys. Chem. **32**, 311 (1981).
[21] B. J. Berne and R. Pecora, *Dynamic Light Scattering* (Wiley-Interscience, New York, 1976).

Downloaded 27 Mar 2001 to 18.60.2.110. Redistribution subject to AIP copyright, see http://ojps.aip.org/jcpo/jcpcr.jsp